Research and verification of the one-step resonance and transport methods based on the OpenMOC code

Chen Zhao[1], Lianjie Wang[1,*]

[1] National Key Laboratory of Nuclear Reactor Technology, Nuclear Power Institute of China, Chengdu, China

ABSTRACT

The one-step method in reactor physics has become one of the important research directions in recent two decades. Based on the open-source OpenMOC code, the following work was carried out. Firstly, the global-local resonance method with multi-group and continuous neutron libraries was researched and established. Next, based on the 2D and 3D MOC solver, the 2D/1D and the MOC/DD transport methods were realized in OpenMOC. Finally, verification of the transport and resonance methods was conducted using the C5G7 macro benchmark and the VERA micro benchmark. The numerical results demonstrated that the average eigenvalue deviation was 44pcm and average maximum pin power distribution deviation was 0.37% in the VERA-2 benchmark, which showed the good accuracy of the resonance method. As for the transport method, 3DMOC method exhibited better accuracy in strong anisotropic cases, but the computational time was 38 times that of the 2D/1D method.

KEYWORDS: One-step method, Resonance, Transport, OpenMOC

1. Introduction

In recent years, with the continuous development of computer technology, the high-fidelity one-step method for precise modeling and calculation of reactors have become one of hotspots in reactor physics research. Several high-fidelity codes have been developed around the world, including DeCART[1], MPACT[2], nTRACER[3], PROTEUS-MOC[4], OpenMOC[5-6], APOLLO-3[7], STREAM[8], NECP-X[9-10], VITAS[11], ALPHA[12]. Research area covers library, resonance, transport, burnup, kinetics and multi-physics coupling, achieving one-step transport calculation for pressurized water reactors.

OpenMOC is an open-source direct transport code with method of characteristics (MOC) developed by the Massachusetts Institute of Technology (MIT). OpenMOC adopts a hybrid programming with Python and C++ languages to balance the good efficiency of C++ and good UI of Python. Constructive solid geometry (CSG) [15] method and long characteristic ray method [16] are applied to support the arbitrary geometry modeling and calculation ability. Spatial domain decomposition parallelism for memory and calculation has been used for large-scale cases. Besides, coarse mesh finite difference (CMFD) for accelerating iterative convergence and GPU/CPU hybrid computing for MOC calculation have been supported in OpenMOC.

In this paper, a resonance module based on the global-local method was added in OpenMOC. Besides, a multi-group library and a continuous library were built for the global-local resonance calculation. In transport module, based on the original 2DMOC and 3DMOC solver, a 2D/1D solver and a MOC/DD solver were expanded. Calculation accuracy and efficiency were compared for the whole-core direct transport method.

2. Framework of the OpenMOC code

The framework of OpenMOC code with added module was shown in Fig.1. Firstly, as for the input/output module, the original structure and input logic were retained, utilizing CSG methods for high-fidelity geometric modeling and incorporating nuclear density input information for addressing real microscopic issues. Next, multi-group and continuous libraries were established for resonance calculation. Then, a global-local resonance calculation module was developed, employing global neutron current method and local pseudo-nuclide subgroup method. Next, inflow transport corrections were applied to obtain macro cross-sections for each material region. Finally, direct transport calculations were performed with 3DMOC, 2D/1D and MOC/DD methods. CMFD and parallel acceleration method were employed from the original OpenMOC code.

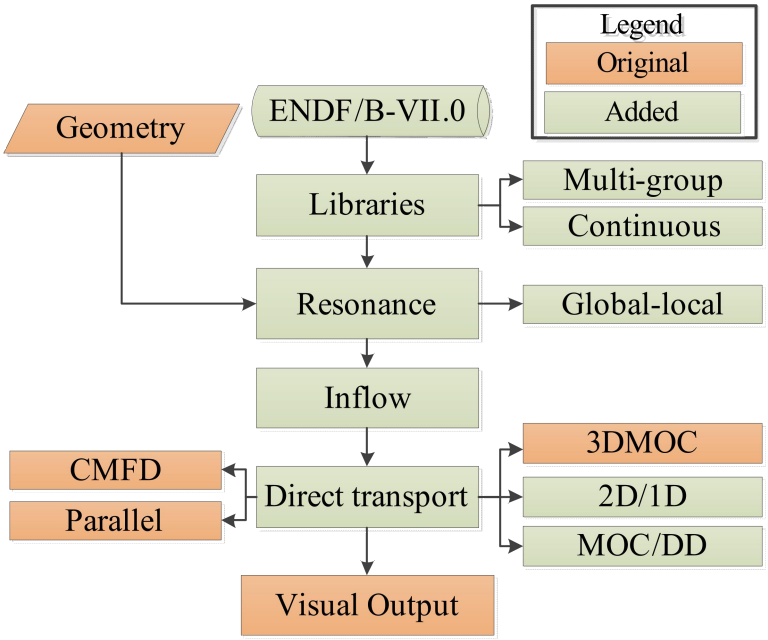

Fig.1 Framework of OpenMOC with added module

3. Global-local resonance method

For the whole-core resonance calculation, the main research approach is to accurately simulate various resonance phenomena while ensuring acceptable computational efficiency. Global-local resonance method separates resonance phenomena into global effects and local effects, balancing computational efficiency and accuracy. It has achieved good computational results in thermal spectrum reactor. The basic theory of global-local method will be divided into libraries, global method and local method.

3.1. Library

This paper continues to use the classical WIMS-69 group structure. Based on the WIMS library, a new multi-group library is expanded to improve the resonance effect calculation capability and a continuous energy library is built to match the global-local resonance method.

1）Multi-group library

For thermal spectrum reactors, the mainstream one-step calculation programs generally use multi-group library energy group structures with less than a hundred groups. Among them, the WIMS database is an internationally renowned open-source library, and its 69-group energy group format is widely used in pressurized water reactor calculations. Based on the WIMS library, improvements have been made in several aspects such as the resonance energy range, resonance nuclides, and resonance integral tables to create a multi-group database suitable for the global-local resonance method.

In terms of resonance energy range, the original resonance range of WIMS is 4eV to 9.118 keV, which cannot consider the resonance peaks of Pu nuclides below 4 eV as shown in Fig. 2. This theoretically causes some deviation in calculation of MOX fuel. Additionally, the ENDF/B-VII.0 evaluated nuclear library provides distinguishable resonance parameters for U-238 above 9.118 keV and the original resonance energy range division did not consider this part of the resonance self-shielding phenomenon. To address the above issues, the multi-group library used in this paper extends the resonance energy range to 0.625 eV~24.78 keV.

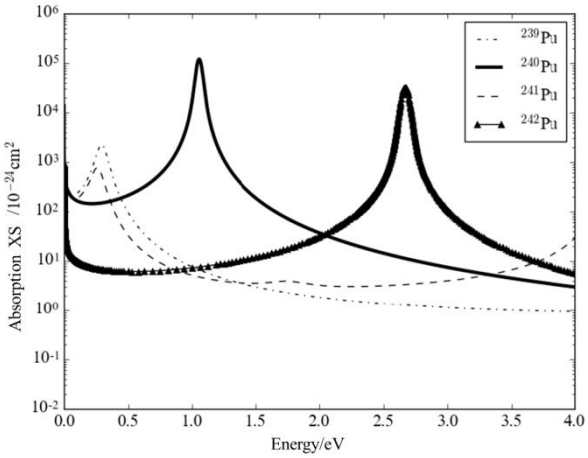

Fig.2 Resonance peak of Pu nuclides in range of thermal energy

Regarding nuclides, ^{242}Pu has a strong resonance effect in the thermal energy region. The WIMS library approximates the resonance self-shielding effect of ^{242}Pu for high-enriched and low-enriched MOX assembly separately. The multi-group library used in this paper expands the resonance energy range, which can explicitly and accurately simulate the resonance peaks of ^{242}Pu. Furthermore, based on the 28 resonance nuclides in the WIMS database, the NJOY program is used to create multi-group databases for Zr, Xe, Sm, Am, Eu, and other nuclides, increasing the number of resonance nuclides to 66.

Besides, the resonance integral tables are expanded in two dimensions: temperature and background cross-section points. The temperature points are increased from 1100K to 1800K and the number of temperature points is increased from 4 to 6. The background cross-section points were limited to 10 by the NJOY program in the original WIMS library. By using the RMET21 program to create resonance integral tables, the number of background cross-section

points is increased to 34. The above improvements further enhance the accuracy of resonance integral table interpolation.

2) library

Considering that the resonance pseudo-nuclide method requires the solution of neutron moderation equations online, an ultra-fine group continuous library is needed. The ultra-fine group cross-section library should include the ultra-fine energy group cross-sections of various nuclides at various temperature points. The amount of data is too large to be stored directly. Therefore, in the continuous energy library, only cross-sections are stored. Using the BROADR module of the NJOY program, the energy points, total cross-sections, elastic scattering cross-sections, fission cross-sections in the output files are processed into binary files. A continuous energy library has been created for 66 resonance nuclides at 32 temperature points. The library size can be decreased to 1.1GB, which is acceptable for storage.

3.2. Global method

In global calculations, for a global system with multiple fuel and moderator regions, after introducing isotropic approximation, the neutron balance equation can be written as follows:

$$\Sigma_f(u)\phi_f(u)V_f = \sum_{f\in F} P_{f'\to f}(u)S_{f'}(u)V_{f'} + \sum_{m\in M} P_{m\to f}(u)S_m(u)V_m \tag{1}$$

Where f is the index of the fuel region; m is the index of the moderator region; $\Sigma(u)$ is the macroscopic cross-section; $\phi(u)$ is the neutron flux density; V is the fuel and moderator density; $S(u)$ is the neutron source; $P_{f'\to f}(u)$ is the probability of isotropic neutrons produced in fuel region f' undergoing their first collision in fuel region f; $P_{m\to f}(u)$ is the probability of isotropic neutrons produced in moderator region m undergoing their first collision in fuel region f.

By introducing the reciprocity relation, neglecting the global resonance interference effects and global temperature distribution effects, and employing a narrow resonance approximation for the source term in the moderator region, the neutron balance equation can be simplified as follows:

$$\Sigma_f(u)\phi_f(u) = \left[1-P_{f\to M}(u)\right]S_f(u) + P_{f\to M}(u)\Sigma_f(u) \tag{2}$$

Assuming there is only absorption and no scattering in the fuel region, and the source term is zero, the equation can be simplified as Eq.(3).

$$P_{f\to M}(u) = \phi_f(u) \tag{3}$$

Introducing the isolated rod approximation to place the fuel rod in an infinitely large moderator, the escape probability $P_e(u)$ equals to the collision probability from fuel to moderator $P_{f\to M}(u)$. Let the flux in the isolated rod fuel region be $\phi_{f,0}(u)$ and the flux in the original system fuel region be $\phi_{f,1}(u)$, the gray dancoff correction factor can be obtained:

$$C_f(u) = \frac{P_{e,f}(u) - P_{f\to M}(u)}{P_{e,f}(u)} = \frac{\phi_{f,0}(u) - \phi_{f,1}(u)}{\phi_{f,0}(u)} \tag{4}$$

To avoid the complexity of grey-dancoff calculation introduced by the energy terms and further reduce computational amount, the concept of black dancoff factor is introduced. Through theoretical derivation of the collision probability $P_{f\to M}(u)$, the calculation formula can be obtained as follows:

$$P_{f\to M}(u)=P_{\mathrm{e}}(u)\left\{1-\frac{C_{\mathrm{b}}\bar{l}\Sigma_f(u)P_{\mathrm{e}}(u)}{1-C_{\mathrm{b}}\left[1-\bar{l}\Sigma_f(u)P_{\mathrm{e}}(u)\right]}\right\} \tag{5}$$

Where $\bar{l}$ is the average chord length of fuel region, $P_{\mathrm{e}}(u)$ is the escape probability, and C_{b} is black dancoff factor. It can be observed that the consistence of $P_{f\to M}(u)$ will be ensured if the black dancoff factor is conserved for the fuel and moderator system. Therefore, as for the entire problem to be solved, black dancoff factors for each pin cell need to be solved for establishing an equivalent one-dimensional model. By introducing the black body approximation, where the cross-section of fuel region is infinitely large, the black dancoff factor can be obtained as:

$$\lim_{\Sigma_f\to\infty} C_{\mathrm{b}}=\lim_{\Sigma_f\to\infty}\frac{P_{\mathrm{e}}-P_{f\to M}}{P_{\mathrm{e}}}=\frac{\phi_{f,0}-\phi_{f,1}}{\phi_{f,0}} \tag{6}$$

In practical calculations, considering the above black body approximation, corresponding cross-section values are set to solve the single-group fixed source equation on a global scale, obtaining the average flux $\phi_{f,1}$ for each fuel rod in the fuel region. For each fuel rod, considering the isolated rod approximation in an infinitely large moderator, the Carlvik method is used to calculate the first collision probability $P_{f\to M}$, denoted as $\phi_{f,0}$. In this way, the black dancoff factor for each fuel rod can be calculated in global calculation.

3.3. Local method

Based on gray dancoff factors obtained from global calculations, an equivalent one-dimensional model is established as shown in Fig.3. This transformation enables the conversion of global calculations into local calculations for individual fuel rods.

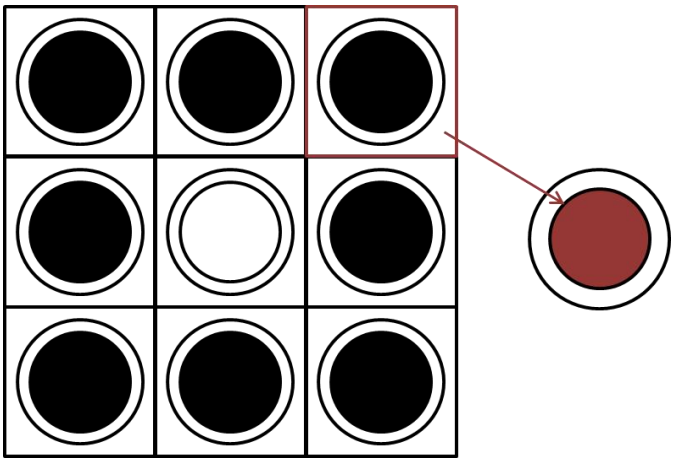

Fig.3 The equivalent one-dimensional model in local calculation

Firstly, searches for the moderator radius of each fuel rod in the one-dimensional model are conducted based on dancoff factors. Maintaining the fuel radius and fuel escape probability P_e constant according to Eq.6, a binary search is employed to compute the collision probability for various moderator radii, aiming to find the moderator radius that aligns with the pin-cell dancoff factor.

Next, all resonance nuclides are transformed into a pseudo-nuclide based on nuclear density ratios. Pseudo-nuclide cross-section tables and subgroup probability tables are established online for each equivalent one-dimensional model. As for the pseudo-nuclide cross-section tables, the total cross-section, absorption cross-section, and scattering cross-section under various state points are calculated with zero-dimensional ultrafine-energy-group method. Input parameters of the interpolation table include background cross-sections, actual temperatures, average temperatures, and burnup depths, as shown in Eq.7. As for the subgroup probability table, subgroup parameters such as the number of subgroups and subgroup cross-sections are determined using the Padé approximation and fitting method for pseudo-nuclides.

$$\sigma_{x,g} = f_{x,g}\left(\sigma_0, T, T_{\mathrm{ave},g}, Bu\right) \tag{7}$$

Subsequently, traditional subgroup methods are employed to solve each equivalent one-dimensional model. This involves establishing subgroup fixed source equations based on subgroup parameters, solving for subgroup flux using collision probability methods, and calculating effective self-shielding cross-sections.

Finally, the SPH factor method is utilized to address multi-group equivalent effects. Iterative processes are conducted to iteratively correct the effective self-shielding cross-sections until convergence is achieved for final SPH factors.

4. Direct transport method

For direct one-step transport calculations, the MOC method has become the mainstream because of excellent geometric description capability and good computational accuracy. Several techniques have been developed based on the MOC method, including the 3DMOC method, the 2D/1D method and the axial expansion method (MOC/DD).

The 3DMOC method directly extends the MOC method into three-dimensional space for accurate solutions. It is considered the ultimate method for direct transport calculations. However, it suffers from low computational efficiency and high memory consumption. The 2D/1D method introduces approximations to transform three-dimensional characteristic rays into multi-layer two-dimensional rays, significantly improving computational efficiency. However, it encounters instability issues and accuracy problems on strong anisotropic cases. The MOC/DD method also transforms three-dimensional characteristic rays into multi-layer two-dimensional rays, while introducing differential relationships along the axial direction to eliminate leakage term isotropic approximations.

Based on the existing two-dimensional MOC calculation module in the OpenMOC program, new modules for the 2D/1D method and the MOC/DD method have been developed. The existing coarse mesh finite difference (CMFD) acceleration method and spatial domain decomposition

parallelization techniques have been retained to enhance the computational capabilities of direct transport calculations.

5. Numerical results

5.1. Macro C5G7 benchmark

C5G7[20] is a mainstream benchmark for validating heterogeneous transport calculation codes, including unrodded, half-rodded (rodA) and fully-rodded (rodB) configurations. For the unrodded case of the C5G7 benchmark, sensitivity analyses of computational parameters were conducted separately for the 2D/1D method and the 3DMOC method. Calculations were performed using the same set of computational parameters for the 3DMOC method, the 2D/1D method and the MOC/DD method.

1）Sensitivity analysis of computational parameters

As for the 2D/1D method, parameters such as ray width, number of azimuthal and polar angle, number of reflector and fuel cell flat source regions, and axial layer height. Sensitivity analysis results were shown in Tab.1. Ray width was analyzed with cases 1~3. Number of angles was analyzed with cases 2, 4, 5. Reflector and fuel flat source region divisions were analyzed with cases 4, 6, 7 and cases 6, 8, 9 separately. Axial layer height was analyzed with cases 8, 10, 11. According to these sensitivity analyses, it can be concluded that the influence of input parameters was relatively small and the maximum deviation from the reference solution was only 63 pcm on case 10. Input parameters, especially the reflector flat source region division, had a more significant impact on pin power distribution results. The maximum pin power difference was improved from 4.30% to 2.96% with refinement of reflector flat source region in cases 4, 6, 7. The default parameters for subsequent calculations were set to be: 0.03cm ray width, 32 and 6 azimuthal and polar angles, 100 and 32 flat source regions for moderator and fuel pin cells, and 3.57cm axial height.

Tab.1 Sensitivity analyses of the 2D/1D method for the C5G7 unrodded case

Cases	Input parameters					k_{eff}	PinPower Max diff	PinPower RMS diff
	Ray width	Azi/pol angles	Reflector FSRs	Fuel FSRs	Axial height			
1	0.05cm	32/6	10*10	4*8	3.57cm	1.14297	2.96%	1.01%
2	0.03cm	32/6	10*10	4*8	3.57cm	1.14296	2.94%	1.01%
3	0.01cm	32/6	10*10	4*8	3.57cm	1.14296	2.94%	1.01%
4	0.03cm	64/6	10*10	4*8	3.57cm	1.14318	2.96%	1.03%
5	0.03cm	128/6	10*10	4*8	3.57cm	1.14338	2.96%	1.04%
6	0.03cm	64/6	8*8	4*8	3.57cm	1.14324	3.63%	1.17%
7	0.03cm	64/6	5*5	4*8	3.57cm	1.14331	4.30%	1.36%
8	0.03cm	64/6	8*8	4*16	3.57cm	1.14328	3.56%	1.15%
9	0.03cm	64/6	8*8	6*16	3.57cm	1.14329	3.56%	1.15%
10	0.03cm	64/6	8*8	4*16	7.14cm	1.14366	3.28%	1.08%
11	0.03cm	64/6	8*8	4*16	1.785cm	1.14323	3.63%	1.17%

As for the 3DMOC method, based on the default parameters from the 2D/1D method, sensitivity analyses were conducted, including the polar ray spacing, axial layer height, linear source method, number of angles. Results were shown in Tab.2. Polar ray spacing needs to be 0.75cm in cases 1-3. Axial height needs to be less than 1.428cm in cases 3-5. Number of angles has little influence in case 2,7. Therefore, the default calculation parameters were set to be: 0.75cm polar ray spacing, 0.714cm axial height and with linear source method.

Tab.2 Sensitivity analyses of the 3DMOC method for the C5G7 unrodded case

Cases	Input parameters				k_{eff}	PinPower Max diff	PinPower RMS diff
	Polar ray spacing	Axial height	Linear source	Azi/pol angles			
1	1.5cm	0.714cm	Yes	32/6	1.14287	7.23%	2.23%
2	0.75cm	0.714cm	Yes	32/6	1.14277	2.57%	0.91%
3	0.25cm	0.714cm	Yes	32/6	1.14276	2.25%	0.82%
4	0.25cm	1.428cm	Yes	32/6	1.14279	2.18%	0.73%
5	0.25cm	3.57cm	Yes	32/6	1.14309	4.02%	0.98%
6	0.25cm	0.714cm	No	32/6	1.14287	3.64%	1.24%
7	0.75cm	0.714cm	Yes	64/6	1.14290	2.60%	0.95%

2）Results of the C5G7 benchmark with three direct transport methods

Based on the sensitivity analyses of calculation parameters mentioned above, the validation calculation of the C5G7 benchmark was conducted with the 3DMOC method, the 2D/1D method and the MOC/DD method. All cases were calculated with 162 CPUs and results were shown in Tab.3.

In terms of calculation accuracy, as for unrodded and rodA cases, eigenvalue and pin power differences were similar. Eigenvalue differences were less than 50 pcm and maximum pin power were less than 3%. All three methods demonstrated good calculation accuracy. As for the RodB case with the strong angular anisotropic effect, the 3DMOC method showed better accuracy performance on the pin power results, reducing the maximum difference from 2.27% to 1.71%.

Regarding the calculation efficiency, the average calculation time for the 3DMOC method was 11331s, which is 38 times longer than the average time 298s for the 2D/1D method and 8.7 times longer than the 1298s for the MOC/DD method. The outer iteration times of the 2D/1D method are 2.50 times of the 3DMOC method and 1.77 times of the MOC/DD method. The phenomenon showed the poor convergence performance of the 2D/1D method, which is caused by the 2D and 1D iteration procedure.

Tab.3 Results of the C5G7 benchmark with three direct transport methods in OpenMOC

	3DMOC	2D/1D	MOC/DD
	Unrodded		
Eigenvalue difference	-27pcm	-32pcm	-17pcm

Pin power RMS difference	0.91%	0.83%	1.04%
Pin power MAX difference	2.57%	2.32%	2.86%
Calculation time	11323s	314s	1281s
Outer iteration times	33	85	47
	RodA		
Eigenvalue difference	-2pcm	-28pcm	-19pcm
Pin power RMS difference	0.80%	0.78%	1.02%
Pin power MAX difference	2.14%	2.14%	2.79%
Calculation time	11305s	295s	1289s
Outer iteration times	33	85	47
	RodB		
Eigenvalue difference	40pcm	-35pcm	-25pcm
Pin power RMS difference	0.64%	0.77%	0.98%
Pin power MAX difference	1.71%	2.27%	2.90%
Calculation time	11364s	284s	1323s
Outer iteration times	34	85	48

5.2. Micro VERA-1 benchmark

Geometric and material parameters for VERA benchmark problems are all derived from the Watts Bar pressurized water reactor nuclear power plant. VERA-1 is a series of pin-cell benchmarks with 5 cases. The VERA-1 benchmark was conducted for validating the global-local resonance module added in the OpenMOC code. Calculation conditions of OpenMOC included 0.01 cm ray spacing, 64 azimuthal angles and 6 polar angles. Eigenvalue results were shown in Tab.4.

Tab.4 Eigenvalue results of the VERA-1 benchmark with OpenMOC

Cases	Description	Keff(KENO-VI)	Keff(OpenMOC)	Keff difference/pcm
1A	Fuel,565K	1.18704±5cpm	1.18734	30
1B	Fuel,600K	1.18215±7cpm	1.18247	32
1C	Fuel,900K	1.17172±7cpm	1.17187	15
1D	Fuel,1200K	1.16260±7cpm	1.16281	21
1E	IFBA,600K	0.77170±7cpm	0.77073	-97

5.3. Micro VERA-2 benchmark

VERA-2 is a series of lattice benchmarks with cases 2A to 2Q in the VERA benchmark package. Descriptions and OpenMOC results were shown in Tab.5. Ray spacing were set to be 0.03cm in all cases except for 0.01cm in IFBA cases. The average eigenvalue difference of the VERA-2 benchmark was 44 pcm. The average maximum and RMS differences were 0.37% and 0.10% separately. Except for the 2H case with 24 B_4C absorber rods, all eigenvalue results were less than 120 pcm. Except for 2O, 2P cases with Gd absorber rods, the maximum pin power

difference was less than 0.6%. All these results showed good accuracy of the newly-developed global-local resonance module in OpenMOC.

Tab.5 Eigenvalue and pin power results of the VERA-2 benchmark with OpenMOC

Cases	Description	Keff (KENO-VI)	Keff (OpenMOC)	Keff diff/ pcm	Pin power diff Max/%	Pin power diff RMS/%
2A	565K	1.18218±3cpm	1.18268	50	0.20	0.07
2B	600K	1.18336±3cpm	1.18392	56	0.18	0.05
2C	900K	1.17375±3cpm	1.17430	55	0.16	0.05
2D	1200K	1.16559±3cpm	1.16604	45	0.15	0.05
2E	600K,12Pyrex	1.06963±2cpm	1.07051	88	0.17	0.04
2F	600K,24Pyrex	0.97602±3cpm	0.97692	90	0.23	0.07
2G	600K,24AIC	0.84770±3cpm	0.84653	-117	0.36	0.13
2H	600K,24B4C	0.78822±3cpm	0.79153	331	0.54	0.14
2I	Instrument,600K	1.17992±2cpm	1.18044	52	0.19	0.05
2J	Instrument,900K,24Pyrex	0.97519±3cpm	0.97617	98	0.20	0.07
2K	Zoned,1200K, 24 Pyrex	1.02006±3cpm	1.02112	106	0.24	0.07
2L	80IFBA	1.01892±2cpm	1.01860	-32	0.28	0.07
2M	128IFBA	0.93880±3cpm	0.93855	-25	0.23	0.07
2N	104IFBA, 20WABA	0.86962±3cpm	0.86926	-36	0.29	0.08
2O	12Gd	1.04773±2cpm	1.04788	15	1.03	0.18
2P	24Gd	0.92741±2cpm	0.92759	18	1.20	0.29
2Q	Zircaloy Grid	1.17194±2cpm	1.17143	-51	0.57	0.14
Average				44	0.37	0.10

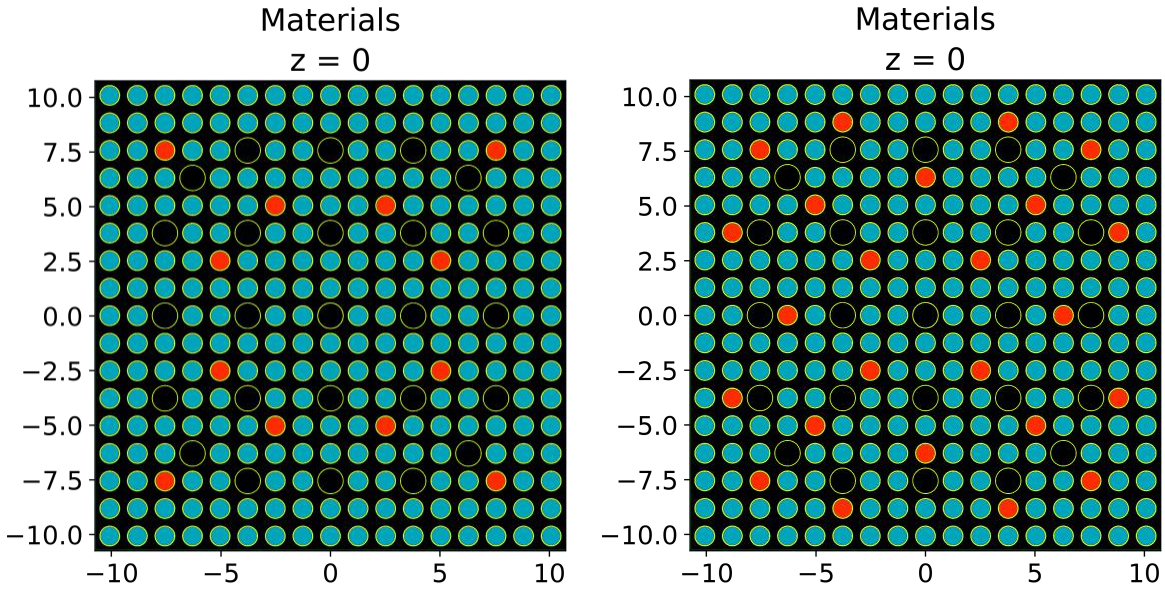

Fig.4 Geometry modeling of Gd absorber cases

To further study the larger eigenvalue and pin power differences on B_4C and Gd absorber cases, results of 2O and 2P cases with Gd absorber were analyzed. The geometry modeling of these two cases was shown in Fig.4, where the red rod was burnable absorber. The detailed pin power differences were shown in Fig.5-6. It can be concluded that the global-local resonance method

undervalued the pin power results of burnable absorber rod, which needs further research in numerical algorithm.

-0.16	-0.07							
-0.18	-0.01	0.17						
	-0.24	-0.13						
0.00	0.08	-1.03	-0.08	0.23				
-0.09	-0.07	0.09	-0.23	0.03				
	-0.10	0.01		0.15	0.05	-0.97		
-0.10	0.05	0.12	0.02	0.09	-0.11	0.18	0.00	
0.00	0.06	0.02	0.01	0.06	0.04	0.17	0.13	0.15

Fig.5 Detailed pin power difference results of the VERA-2O case/%

-0.28	-0.18							
-0.01	0.03	-1.10						
	-0.29	-0.08						
-0.05	-0.04	0.13	0.02	-1.15				
-1.20	0.12	0.13	-0.23	0.06				
	-0.15	-0.15		0.20	0.05	-1.06		
-0.02	0.14	0.16	-1.06	0.23	0.05	0.25	0.07	
-0.09	0.01	-0.09	0.21	0.04	0.12	0.26	0.13	0.16

Fig.6 Detailed pin power difference results of the VERA-2P case/%

6. Conclusion

Based on the OpenMOC open-source MOC transport calculation code, the global-local resonance method and direct transport methods were researched. A resonance calculation module, as well as multi-group and continuous-energy libraries, was developed in the framework of OpenMOC to provide multi-group cross-sections. A direct transport module with the 3DMOC method, 2D/1D method and the MOC/DD method was developed to provide multiple choices for calculation. Macro C5G7 benchmark and micro VERA benchmark were applied for the validation and calculation performance comparisons. As for the macro C5G7 benchmark, three kinds of direct transport method were compared for the accuracy and efficiency with a code system. Numerical results showed the better accuracy of the 3DMOC method on stronger anisotropic cases. However, the computation time for the 3DMOC was 38 times longer than that of the 2D/1D method. As for the VERA benchmark, average eigenvalue and maximum pin power differences were 44 pcm and 0.37%, which showed the good accuracy of resonance method. The resonance method can provide accurate multi-group cross-sections for the OpenMOC direct transport solver.

ACKNOWLEDGMENTS

This work is supported by Foundation of Nuclear Power Institute of China.

REFERENCES

1. H. Mathieu. Full Core, Heterogeneous, Time Dependent Neutron Transport Calculations with the 3D Code DeCART. Berkeley, USA: University of California at Berkeley, 2010.
2. Collins B, Kochunas B, Jabaay D, et al. Verification of MPACT: Michigan parallel characteristics transport code. Transactions of the American Nuclear Society 108:795-798 • January 2013.

3. N. Choi, H. Park, H. Lee et al. Recent Capability and Performance Enhancements of the Whole-core Transport Code nTRACER. PHYSOR2020, Cambridge, United Kingdom, Mar.29-Apr.2, 2020.
4. Y. Jung, C. Lee. Performance Improvement of the Linear System Solver for CMFD Acceleration in PROTEUS-MOC. Transactions of the American Nuclear Society, Minneapolis, USA, June 9–13, 2019.
5. W. Boyd. Massively parallel algorithms for method of characteristics neutral particle transport on shared memory computer architecures. USA, Massachusetts Institute of Technology, 2014.
6. G. Gunow. Full Core 3D Neutron Transport Simulation Using the Method of Characteristics with Linear Sources. USA, Massachusetts Institute of Technology, 2018.
7. D. Schenider, F. Dolci, F. Gabriel et al. APOLLO3® : CEA/DEN Deterministic Multi-Purpose Code for Reactor Physics Analysis. PHYSOR 2016, Sun Valley, ID, May 1–5, 2016.
8. S. Choi, J. Choe, K. Nguyen et al. Recent Development Status of Neutron Transport Code STREAM. Transactions of the Korean Nuclear Society Spring Meeting Jeju, Korea, May 23-24, 2019.
9. C. Zhao, Z. Liu, Y. Zheng, et al. Improved leakage splitting method for the 2D/1D transport calculation. Progress in Nuclear Energy, 2018, 105:202-210.
10. Z. Liu, Q.He, T. Zu et al. The pseudo-resonant-nuclide subgroup method based global–local self-shielding calculation scheme. Journal of Nuclear Science and Technology, 55:2, 217-228, 2018.
11. T. Zhang, W. Xiao, H. Yin. VITAS: A multi-purpose simulation code for the solution of neutron transport problems based on variation nodal methods. Annals of Nuclear Energy, 2022, July, 178, 109335.
12. Z. Hang, Q. Zhang, L. Liang et al. Investigation on the modeling capability of ALPHA code for fuel rod deformation. Annals of Nuclear Energy, Vol.169, May 2022, 108892.
13. Y. Liu, B. Collins, B. Kochunas et al. Resonance self-shielding methodology in MPACT. M&C 2013, Sun Valley, Idaho, May 5-9, 2013.
14. S. Choi, D. Lee. Three-dimensional method of characteristics/diamond-difference transport analysis method in STREAM for whole-core neutron transport calculation. Computer Physics Communications, 260, 107332, 2021.
15. L. Cao, Z. Liu, L. Cao et al. Implementation and Application of the CSG Method in the NECP-X Code. Proceedings of ICONE-27, 27th International Conference on Nuclear Engineering, May 19-24, 2019, Ibaraki, Japan.
16. Suslov I. Improvements in the long characteristics method and their efficiency for deep penetration calculations[J]. Progress in Nuclear Energy, 2001, 39(2): 223-242.
17. Sugimura, N., Yamamoto, A., 2006. Evaluation of dancoff factors in complicated geometry using the method of characteristics [J]. J. Nucl. Sci. Technol. 43 (10), 1182–1187.
18. S. Stimpson, M. Young, B. Collins et al. Assessment and Improvement of the 2D/1D Method Stability in DeCART. M&C 2013, Sun Valley, Idaho, May 5-9, 2013.
19. Y. Zheng, S. Choi, D. Lee. A new approach to three-dimensional neutron transport solution based on the method of characteristics and linear axial approximation. Journal of Computational Physics, 350(2017): 25–44.
20. OECD, “Calculations Without Spatial Homogenization. MOX Fuel Assembly 3-D Extension Case”, Nuclear Science, NEA/NSC/DOC(2005)16.